Experimental Results for Adaptive Radar Imaging in a Wide Angular Sector

Mark Curry and Yasuo Kuga

Department of Electrical Engineering
University of Washington, Box 352500
Seattle, WA 98195-2500

Abstract - We investigate experimentally, an adaptive imaging approach, namely that of a synthetic wideband, stepped CW transmitter and a multichannel, adaptive array for receiving backscattered energy from short range objects in a full +/- 90 degree field of view. The method is a hybrid one, using conventional Fourier processing for range and is adaptive in angle. The 12 element linear array that was constructed is able to form an image in range and angle without Doppler information, and was tested with targets embedded in natural background clutter. The results show how background clutter affects the angular resolution of the array due to the increase in rank of the signal plus clutter covariance matrix, whereas at the same time the rank of this matrix is reduced for closely spaced scatterers due to signal coherence. In addition to investigating some known angular enhancement methods, we propose a method to enhance angular resolution in the presence of clutter by a projection, which seeks to reduce the received signal to a lower rank approximation, without using eigendecomposition, thus having an implementation advantage. This method allows more control over the angular resolution and the background clutter level. Computer simulations as well as the experimental results are presented.

I. INTRODUCTION

Fig. 1 shows the scenario for microwave imaging. Although we are imaging simple objects in an anechoic chamber, *anechoic* is somewhat misleading since the integrated backscattered field from the chamber is high enough to exhibit structure and is not uniform spatially.
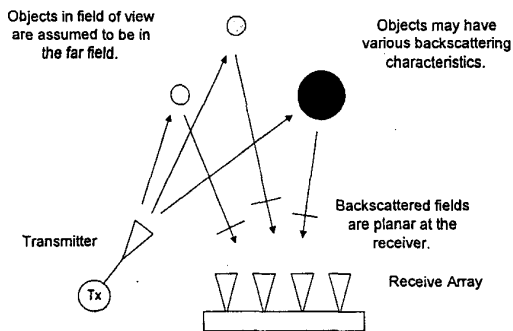

Fig. 1. Microwave Imaging Arrangement

Range resolution is achieved by synthetic-wideband, stepped CW signals. In our previous work [1], [2] we discussed a four- channel array operating at about 1 GHz. These results were encouraging enough to construct a new system with 12 wideband elements operating at 2.5 GHz. Reference [3] recently reported results using a similar basic approach with an experimental adaptive array, employing FM chirp in an outdoor environment. In our work we have emphasized the need for proper compensation for dispersion so that imaging over a wide angular sector will be near optimal. Our technique has some similarities to superresolution SAR imaging [4], [5], [6], [7], however in our case the aperture consists of only the single set of elements on the array itself and covers a wide angular sector. In addition, the clutter statistics will be very different due to a non-uniform spatial clutter distribution.

II. SIGNAL MODEL

First we review the angular array geometry and the array outputs for wideband signals. Consider a superposition of fields backscattered from objects in the field of view of the transmitter. Assume objects are in the far field so the plane wave assumption is valid. The incident plane waves can be parameterized by their angle of arrival as shown in Fig. 2.
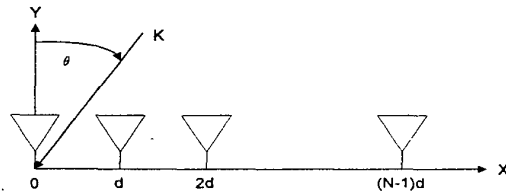

Fig. 2. Uniform Linear Array Geometry

The baseband antenna output for frequency m and element n, for *Ntargs* scatterers at range r_i and angle θ_i is

$$V_o(n,m) = \sum_{i=1}^{i=Ntargs} e^{-j2\pi m\Delta f \frac{2r_i}{c_o}} e^{-j2\pi \frac{f_o}{c_o} nd \sin\theta_i} e^{-j2\pi (\frac{m}{M}-\frac{1}{2})\frac{f_{BW}}{c_o} nd \sin\theta_i} \quad (1)$$

Transmit frequency, $f_m = f_o + (m - M/2)\Delta f$ and f_o is the center frequency of the antenna. The first exponential term describes the phase information for range, and the second and third terms describe the inter-element phase due to the incidence angle. The second term describes the linear phase shift across the array for incidence angle θ_i, which is independent of frequency. However the third term shows an additional phase across the array which is dependent on frequency $m\Delta f$. The affect of the last term is to cause the angle of arrival to appear to change as the incident field wavelength changes (dispersion). The angular sweep is proportional to the true angle. For large angles of arrival the angular broadening is greatest. We can remove the angular dispersion effect and not interfere with range phase information if we do not alter the antenna phase center. This requirement is met by using spatial resampling to map the incident fields to the narrowband plane wave model. For our hybrid approach we have chosen to perform the range compression using a zero-padded FFT on each focussed array element output. Then each range bin contains the superposition of target plane wave responses for all targets at the same range. Using a conventional approach for range compression allows for a minimum of target shape constraints in the range dimension. For example a target does not have to be point-like in the range dimension. This relaxes the model requirements somewhat. We use adaptive beamforming in the angle dimension to achieve timproved resolution from a small antenna.

III. SPATIAL RESAMPLING

The array outputs must be properly focussed so that the angle of arrival of a single plane wave is constant for a given frequency m. This is equivalent to saying that the signal model is low rank, i.e. parameterized by the angle of arrival only. One method for focussing involves resampling the array outputs to correct for the constant element spacing d. See [8] for discussion of spatial resampling techniques applied to wideband angle of arrival estimation for uncorrelated signals. The resampling process creates a set of data at finely spaced intervals that allows samples at varying distances from the antenna phase center to be extracted. Due to dispersion, as the frequency m increases, the distance d appears to increase, as far as angle of arrival is concerned, so to offset this affect we extract samples closer to the center of the interpolated array. Conversely as the frequency decreases we must extract samples farther from the array center. The focussing procedure can be derived by combining the 2nd and 3rd exponential terms from (1) and then set $\Delta f = f_{BW}/M$. Then recall that f_o is the center frequency of the array to yield the following expression for the array output

$$V_o(n,m) = \sum_{i=1}^{i=Ntargs} e^{-j2\pi m\Delta f \frac{2r_i}{c_o}} e^{-j2\pi\left(\frac{f_o}{c_o}+\left(m-\frac{M}{2}\right)\left(\frac{\Delta f}{c_o}\right)\right)nd\sin\theta_i} \quad (2)$$

We then extract the frequency dependent part of the 2nd term and equate this to an array with constant frequency and variable spacing d_f to yield

$$d\left(\frac{f_o}{c_o}+\left(m-\frac{M}{2}\right)\left(\frac{\Delta f}{c_o}\right)\right) = d_f\frac{f_o}{c_o} \quad (3)$$

where d is the physical spacing between elements. Solve for d and then note that the largest value of d occurs at the lowest array frequency f_{min}. This result is given by

$$\left\{\left(\frac{d_f f_o}{c_o}\right)\Big/\left(\frac{f_{min}}{c_o}\right)\right\} \le d_o \quad \therefore \quad d_f \le \frac{d_o f_{min}}{f_o} \quad (4)$$

where d_o is the true physical separation between elements. While it is possible to extrapolate beyond the ends of the array, a potentially large error must be accepted since the values are assumed to be zero outside the array. It is possible to use a model-based approach to help in the extrapolation, however this has not been found to improve the angular resolution or increase the number of resolvable targets. We set the inequality in (4) to an equality so that the array is as large as possible for maximum angular resolution. Next we combine the terms and derive the focussed array output. By setting

$$d = \frac{d_o f_o (f_{min}/f_o)}{\left(f_o + (m-M/2)\Delta f\right)} \quad (5)$$

in (6), we see the focussed array yields the correctly transformed output to generate a superposition of narrowband plane waves at ranges r_i and angles θ_i

$$V(m,n) = \sum_{i=1}^{i=Ntargs} e^{-j2\pi m\Delta f 2\left(\frac{r_i}{c_o}\right)} e^{-j2\pi\left(\frac{f_o}{c_o}\right)nd_o\left(\frac{f_{min}}{f_o}\right)\sin\theta_i} \quad (6)$$

This result has the desired properties to employ narrowband adaptive beamforming techniques in an optimal way, namely a superposition of plane waves. We observe that since the effective array spacing has been modified by $\beta = f_{min}/f_o$ we will modify the steering vectors by the same amount when we do adaptive beamforming so that the angle of a target response is correct. Note that the transformation in (6) will

focus all targets at all ranges since the focussing procedure is independent of range. Next, we describe the procedure for interpolating the array, so samples at the desired spacing may be obtained.

The resampling is accomplished by approximating a continuous array by interpolation of the given data and then extracting the required samples at the new sampling interval required for each temporal frequency m. Interpolation is accomplished by inserting K-1 zeros between samples, where K is the interpolation factor, to produce a vector of length KN. A least-squares interpolation filter is applied to the data. Once the array output has been interpolated we extract N samples with the proper spacing. For an interpolated array of length KN we may rewrite (6) to yield the index into the interpolated array for element n, and frequency m, as

$$Y(n,m) =$$
$$X_{int}\left(rnd\left(\left(\frac{KN+1}{2} \right) + \frac{MK\left(f_{min}/f_o \right)\left(n-N/2 \right)}{M+\left(BW/f_o \right)\left(m-M/2 \right)} \right), m \right) \quad (7)$$

where $X_{int}(*)$ refers to the interpolated data matrix and Y is the focussed data matrix of size M by N, the same size as the unfocussed data. The offsets into the interpolated array are all relative to the array phase center at $(KN+1)/2$. The $rnd(*)$ function serves to extract the closest integer index to the desired one. The $rnd(*)$ function may be replaced by a linear interpolation of the data at the 2 nearest neighbors, however this has not been found to improve performance. As a demonstration of these results, refer to the upper plot of Fig.3 which uses a 128 point, 2D-FFT of synthetically generated FM-CW data for several point targets. The lower portion has been resampled before Fourier processing and has significantly improved resolution at high angles.

IV. ANGULAR SPECTRUM ESTIMATION

This section outlines the minimum variance spectral estimation method used to derive the angular spectrum at each range bin. The data from all bins at the same range are grouped together to form a vector X_m, of N elements. This vector contains the angular information about all targets at the same range. Minimum variance spectral estimation is well known, and straightforward to implement [9]. Starting with the assumed steering vector

$$\vec{s}(\phi) = [e^{j0\phi}, e^{j1\phi}, \dots, e^{j(N-1)\phi}]^T \quad (8)$$

where $\phi = kd\sin\theta$, and θ is the angle of arrival of the incident plane wave. The received power at a particular steering angle is used to form the image and is given by

Beamforming using 2D-FFT, narrowband assumption

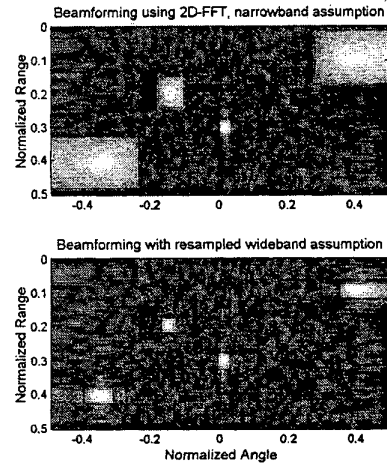Beamforming with resampled wideband assumption

Normalized Angle

Fig. 3 The top image shows a wideband signal for 4 targets that has been converted to the spatial domain by a 2D-FFT, thus assuming a narrowband, plane wave case. In the lower portion we see the targets are now essentially delta functions in range-angle space after resampling and focussing, thus fitting the narrowband plane wave model.

$$P(\phi) = \frac{1}{\vec{s}^H(\phi)\mathbf{R}^{-1}\vec{s}(\phi)} \quad (9)$$

To estimate $\mathbf{R}$ from the available data requires independent and identically distributed (iid) samples of $\mathbf{x}$, the observed data. For the case of image formation as discussed here there are no iid samples for 2 reasons. The stationary scene has no Doppler information, and all targets at the same range, independent of angle, are correlated. It is however possible to combine multiple closely spaced groups of frequencies to mitigate the effects of white noise, such as thermal noise in the receiver. After computing the Fourier transforms of the element signals we may have one single snapshot of data at each range bin from which to derive the angles of arrival of objects at that range.

For correlated signals and linear arrays, sub-array averaging (spatial smoothing) [10], [11], [12] is used to estimate a spatial correlation matrix from as little as one snapshot. After forward spatial smoothing, forward-backward averaging is used to significantly improve the estimate of $\mathbf{R}$. The tradeoff for using spatial smoothing is a smaller effective aperture, which leads to fewer degrees of freedom for beamforming. Additionally, the angular resolution is not nearly as good as that obtained for uncorrelated signals.

One approach for improving the resolution involves squaring the correlation matrix $\mathbf{R}$, before spatial smoothing. See [13] for a discussion of the method and the resolution properties of spatially smoothed correlation matrices. Squaring the correlation matrix increases the robustness of

the dominant eigenvectors, which results in better resolution for closely spaced arrivals. This approach has been found to improve resolution over the spatially smoothed but non-squared approach. It provides consistent AOA estimates, but the variance of target RCS has been found to increase significantly and has a long-tailed distribution. These spatial smoothing methods will be used as a starting point for the experimental work.

V. APPROXIMATE SIGNAL SUBSPACE PROJECTION (ASSP)

The radar background clutter will not in general, fit the low rank signal plus noise model that was outlined earlier. Clutter signals may easily span many degrees in angle. This has been observed in our anechoic chamber and it was found that the signal amplitude returned from the chamber itself has a structure that is relatively strong and repeatable. This clutter is due to constructive interference at the receive array from the integrated field of the periodic structures and many oblique incidence angles to the cones in the chamber. Consequently, the imaging array is readily able to display some structure of the clutter. For targets such as dihedral reflectors about 2-3 wavelengths in size the background clutter is about 15-20 dB below the target return, but is not really homogeneous across all ranges and angles of interest. The idea of ASSP is to increase the signal to clutter plus noise ratio or SCNR by a rank reducing linear operator. We are concerned with the 'effective' rank' so the goal is to increase the robustness of the signal eigenvectors by attenuating the clutter and noise eigenvalues. In the case of correlated signals, if all other variables are held constant, then increasing the signal to noise ratio will improve the resolution. We start with the unitary decomposition of the signal covariance matrix. We assume the noise is white:

$$R = U_s \Lambda_s U_s^H + \sigma^2 U_s U_s^H \qquad (10)$$

The signal component will contain the signal and the clutter, with the clutter subspace associated with the smaller eigenvalues. We wish to estimate a lower effective-rank signal subspace to reduce the clutter contribution without doing an eigendecomposition and estimating the number of signals. While a full eigendecomposition and principal components estimation can be done in extremely high clutter levels, a similar net result can be approximated for low to medium clutter levels using the following linear operator P:

$$P = R^n (R^n + \alpha^n I)^{-1} \qquad (11)$$

If $\alpha \neq 0$, using the unitary decomposition $R = U \Lambda U^H$ yields

$$P = (U \Lambda U^H)^n [(U \Lambda U^H)^n + \alpha^n I]^{-1}$$
$$= U \Lambda^n U^H [U(\Lambda^n + \alpha^n I) U^H]^{-1}$$
$$= U \Lambda^n (\Lambda^n + \alpha^2 I)^{-1} U^H$$
$$= U H_s U^H \qquad (12)$$

$$H_s = \Lambda^n (\Lambda^n + \alpha^n I)^{-1}$$

$$\hat{R} = PR = U H_s U^H U \Lambda U^H = U H_s \Lambda U^H$$

Since Λ^n is diagonal, we may write down the expression for the diagonals of H_s:

$$H_s(i,i) = \frac{\lambda_i^n}{\lambda_i^n + \alpha^n} \quad \begin{cases} H_s(i,i) \to 1 & \text{for } \lambda \gg \alpha \\ H_s(i,i) \to 0 & \text{for } \lambda \ll \alpha \end{cases} \qquad (13)$$

A plot of (13) will show a family of smooth curves between zero and one, depending on choices of α and n. The higher that n is, the more rapid the transition. Values of n that have given good results are typically 2 to 4. The P matrix does not alter the eigenvectors of R, but acts as a nearly linear transfer function for the large eigenvalues of R, depending on their values relative to α. If the value of α is chosen properly then P will act as an approximate projector onto the eigenvectors of R with the largest associated eigenvalues. Matrix P will attenuate the eigenvectors of R with eigenvalues smaller than α. For $n=2$, to square the condition number of matrix PR set

$$\alpha = \sqrt{\lambda_{max} \lambda_{min}} \qquad (14)$$

This effect is somewhat similar to the case of squaring the covariance matrix, but now we have some control of the rank of signal subspace, which allows for discrimination between target signals and background clutter. In order to estimate a value of α we must do a preliminary spectral estimate in order to find the peak signal level and the clutter and noise background level. As an example, consider the angular spectrum, Fig. 4 and the corresponding eigenvalue distribution. The data contains 3 strong signals, 2 of which are relatively closely spaced, and 1 signal at –20 dB relative to the other 3. In this case we have a peak signal to noise level of about 30 dB, with an associated peak eigenvalue to average noise eigenvalue level of about 30 dB. An estimate of α, based on (14) that has worked well in practice is the peak of the spectrum signal power multiplied by the minimum of the spectrum signal power divided by 2*sub-array size. This corresponds to the mean value in dB between the signal peak and noise floor. It's easy to show that this value also has the correct units for α. Once α is chosen we use PR to estimate the resolution enhanced angular spectrum. The improvement in angular resolution and weak signal detection is apparent.
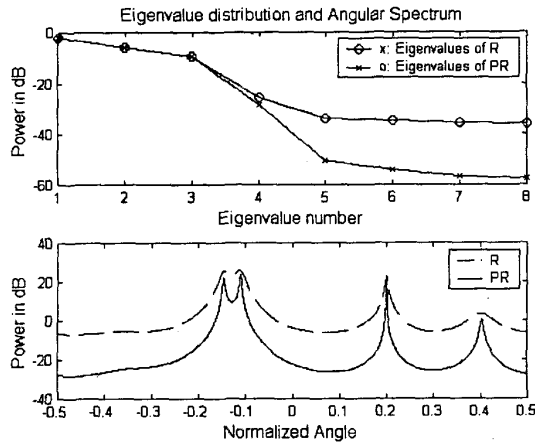
Fig. 4. Comparison of spatial smoothing only and spatial smoothing plus the ASSP technique. ASSP shows a higher signal to noise ratio.

Fig. 6. Imaging array system in anechoic chamber. The linear discone array is seen across the top. The microwave receiver is at the bottom.
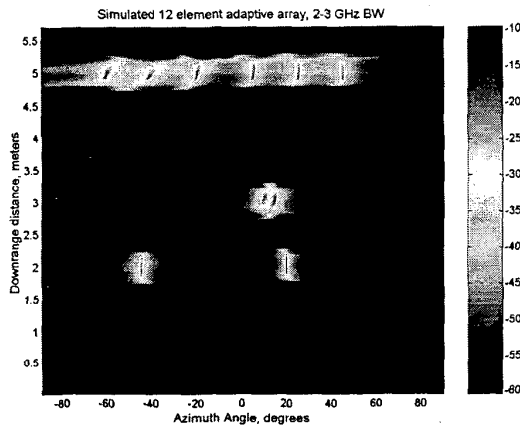

Fig. 5. Simulated 12-element array, using spatial smoothing and ASSP. Two targets at 3m have 5° spacing, with 6 targets at 5m range.

VI. EXPERIMENTAL SYSTEM AND RESULTS

The prototype imaging system uses a wide beamwidth horn antenna for the transmitter that steps from 2-3 GHz in 40 steps at 5dBm. The center frequency is, F_c = 2.5 GHz or 12cm wavelength. The receiver consists of 12 vertically mounted discone antennas, spaced at $\lambda_c/2$ intervals. Discones have worked well for radar imaging. Their properties include a dipole pattern, which is isotropic in azimuth, excellent bandwidth; the units constructed have a –20 dB return loss from 2-4 GHz. An important factor is their phase center, which remains constant over a wide frequency range. Element signals are multiplexed by microwave relays into a 70dB gain, receiver. The RF and transmit reference signals are mixed to 102.5 KHz.
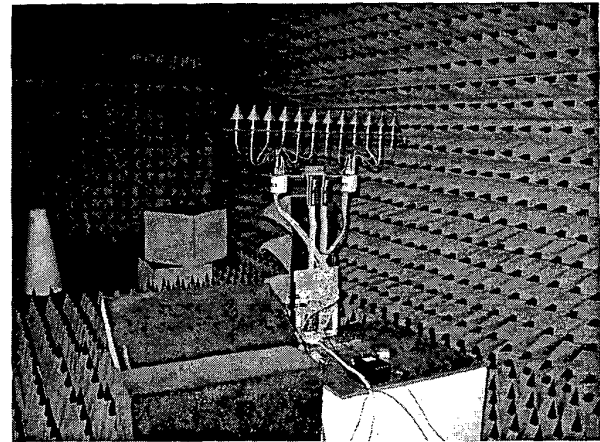
Sampling and S-parameter processing is done with a custom TMS320C25 DSP board. Signals are sampled at 10 KHz with 12 bits of resolution to create a 2.5 KHz discrete time final IF due to undersampling and converted to complex baseband by mixing with digital quadrature oscillators. Low pass filtering is done by integration. The S_{21} estimates for each antenna element are obtained by dividing the complex receive component by the complex transmit component and passed to the PC in floating point format. Fig. 6 shows the chamber setup.

The targets consist of metal cylinders and dihedral reflectors. Object interactions such as multiple scattering have been ignored in these experiments. We have collected many types of images of various configurations, for example some were placed in line extending over some range, and some were placed in front of each other. One particular case is 2 dihedrals placed 7 degrees apart at about 3.5 meters in range. The targets are sitting on a box near the back wall of the chamber. The dihedrals are approximately 75% of a beamwidth apart. Regarding the range, the wavelength is about 12 cm therefore, if we go 10 wavelengths out, that is about 1.2 m away, which just barely qualifies as the far field. Correcting the steering vectors for near-field wave fronts did not improve image quality for ranges greater than 1.5 m., so the far field approximation is reasonable. The useful range of targets in the chamber is about 2-6 meters in range. The background clutter from the chamber is about 15-20 dB below the target returns. In Fig. 7 it is not possible to discern that there are 2 dihedrals, however in the Fig. 8 they are clearly visible. Fig. 8 incorporates spatial smoothing and ASSP. The region at about 3.5m and –20 to +20 degrees contains a row of large, rough but relatively flat objects with intermediate backscattering amplitude. The bright spot at the bottom and about –45° is leakage signal from the transmit

330

antenna itself. Experimentally we have found that clutter may span large angles and does not fit the simple assumed model. When this occurs there is degradation in angular resolution. The ASSP method helps in this regard because the higher the threshold α, the more clutter is suppressed. This can be important when the number of elements is small, as in this case. Fig. 9 shows a case of imaging multiple targets, with 3 cylinders at the same range and a nearby larger reflector.
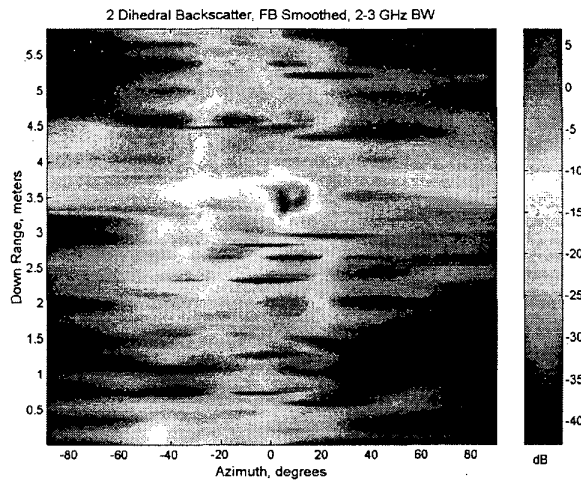

Fig. 9. Sample image of 3 cylinders at the same range and one large corner reflector, the image has been scan converted to meters in both dimension.

demonstrated that after spatial resampling, adaptive beamforming can perform well for RCS imaging of close range objects over large angles, with small antennas. We developed and tested a method called ASSP for improving angular resolution in the presence of spatial clutter.

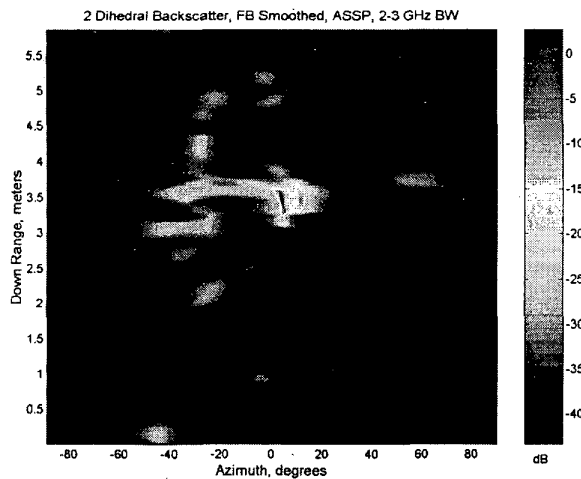**Fig. 7.** Image of 2 dihedral reflectors, spatial smoothing only

Fig. 8. The same 2 dihedral reflectors but includes spatial smoothing and ASSP enhancement. The improvement in angular resolution is apparent as well as de-cluttering the background.

VII. CONCLUSION

We have demonstrated a complete system for performing high-resolution microwave imaging to validate our approach and the results clearly support the ideas. We have
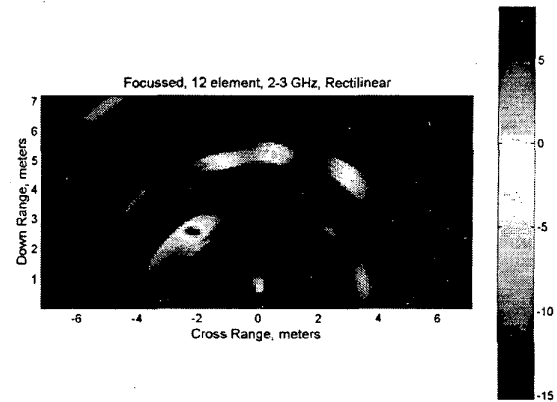
REFERENCES

[1] M. A. Curry and Y. Kuga, "Radar Imaging Using a Wideband Adaptive Array", Adaptive Sensor Array Processing Workshop, MIT Lincoln Laboratory, Lexington, Mass., March, 2000a.
[2] M. A. Curry and Y. Kuga, "Radar Imaging Using a Wideband Adaptive Array", IEEE 2000 International Radar Conf., Washington, DC, May, 2000b.
[3] P. Grahn and S. Bjorklund, "Short Range Radar Measurements using an Experimental Digital Array Antenna", IEEE 2000 International Radar Conf., Washington, DC, May, 2000.
[4] S. DeGraaf, "SAR Imaging via Modern 2-D Spectral Estimation Methods", IEEE Trans. on Image Processing", vol.7, pp. 729-761, 1998.
[5] R. L. Fante, "Adaptive Nulling of Sidelobe Discretes", IEEE Trans. Aero. and Elec. Systems, vol. 35, no. 4, pp. 1212-1218, Oct., 1999.
[6] G. R. Benitz, "High-Definition Vector Imaging",Lincoln Laboratory Journal, vol. 10, no. 2, pp. 147-170, 1997.
[7] S. L. Borison, S. B. Bowling, and K. M. Cuomo, "Super-Resolution Methods for Wideband Radar," Lincoln Laboratory Journal, vol. 5, no. 3, pp. 441-462, 1992.
[8] J. Krolik and D. Swingler, "Focused Wide-Band Array Processing by Spatial Resampling", IEEE Trans. Acoust., Speech, Signal Processing, vol. 38, No. 2, pp. 356-360, 1990.
[9] J. Capon, "High_Resolution Frequency-Wavenumber Spectrum Analysis," Proc. IEEE, vol. 57, no. 8, pp. 1408-1419, 1969.
[10] N. Wiener, "Extrapolation, Interpolation and Smoothing of Stationary Time Series", MIT Press, Cambridge, MA. 1949.
[11] T. J. Shan, A. Paulraj and T. Kailath, "On Spatial Smoothing for direction of arrival estimation of coherent signals, " IEEE Trans. Acoust., Speech, Signal Processing, vol. ASSP-33, pp. 806-811, 1985.
[12] K. J. Raghunath and U. V. Reddy, "Finite data performance analysis of MVDR beamformer with and without spatial smoothing", IEEE Trans. Acoust., Speech, Signal Processing, vol. 40, pp.2726-2736,1992.
[13] J. Li, "Improved Angular Resolution for Spatial Smoothing Techniques", IEEE Trans. on Signal Processing, vol. 40, no. 12, 1992.